Biochimica et Biophysica Acta 896 (1987) 153–164
Elsevier

BBA 73186

Structure and metastability of *N*-lignocerylgalactosylsphingosine (cerebroside) bilayers

Robert A. Reed and G. Graham Shipley

Biophysics Institute, Departments of Medicine and Biochemistry, Boston University School of Medicine, Boston, MA (U.S.A.)

(Received 21 July 1986)

Key words: Cerebroside bilayer; Phase structure; Differential scanning calorimetry; X-ray diffraction

Differential scanning calorimetry (DSC) and X-ray diffraction have been used to study hydrated *N*-lignocerylgalactosylsphingosine (NLGS) bilayers. DSC of fully hydrated NLGS shows an endothermic transition at 69–70°C, immediately followed by an exothermic transition at 72–73°C; further heating shows a high-temperature (T_c = 82°C), high-enthalpy (ΔH = 15.3 kcal/mol NLGS) transition. Heating to 75°C, cooling to 20°C and subsequent reheating shows no transitions at 69–73°C; only the high-temperature (82°C), high-enthalpy (15.3 kcal/mol) transition. Two exothermic transitions are observed on cooling; for the upper transition its temperature (about 65°C) and enthalpy (about 6 kcal/mol NLGS) are essentially independent of cooling rate, whereas the lower transition exhibits marked changes in both temperature (30 → 60°C) and enthalpy (2.2 → 9.5 kcal/mol NLGS) as the cooling rate decreases from 40 to 0.625 Cdeg/min. On reheating, the enthalpy of the 69–70°C transition is dependent on the previous cooling rate. The DSC data provide clear evidence of conversions between metastable and stable forms. X-ray diffraction data recorded at 26, 75 and 93°C show clearly that NLGS bilayer phases are present at all temperatures. The X-ray diffraction pattern at 75°C shows a bilayer periodicity d = 65.4 Å, and a number of sharp reflections in the wide-angle region indicative of a crystalline chain packing mode. This stable bilayer form converts to a liquid-crystal bilayer phase; at 93°C, the bilayer periodicity d = 59.1 Å, and a diffuse reflection at 1/4.6 $Å^{-1}$ is observed. The diffraction pattern at 22°C represents a combination of the stable and metastable low-temperature bilayer forms. NLGS exhibits a complex pattern of thermotropic changes related to conversions between metastable (gel), stable (crystalline) and liquid-crystalline bilayer phases. The structure and thermotropic properties of NLGS are compared with those of hydrated *N*-palmitoylgalactosylsphingosine reported previously (Ruocco, M.J., Atkinson, D., Small, D.M., Skarjune, R.P., Oldfield, E. and Shipley, G.G. (1981) Biochemistry 20, 5957–5966).

Abbreviations: NLGS, *N*-lignocerylgalactosylsphingosine; NPGS, *N*-palmitoylgalactosylsphingosine.

Correspondence: G.G. Shipley, Biophysics Institute, Departments of Medicine and Biochemistry, Housman Medical Research Center, Boston University School of Medicine, 80 East Concord Street, Boston, MA 02118, U.S.A.

Introduction

The lipid bilayer compartment of animal cell plasma membranes is chemically heterogeneous, containing different chemical classes of phospholipids (phosphatidylcholine, phosphatidyleth-

anolamine, phosphatidylserine, etc.) and sphingolipids (sphingomyelin, cerebrosides, gangliosides, etc.), as well as cholesterol. It is further complicated by chain length/unsaturation variations in the glycerol ester-linked and sphingosine amide-linked fatty acids. In most cases, glycosphingolipids such as cerebrosides and gangliosides are present in membranes in relatively small amounts [1], but they appear to be located exclusively in the extracellular monolayer of the membrane [2]. The sugar component of glycosphingolipids may be functionally important and either endow the cell surface with recognition properties or be involved in receptor-mediated process (for a review, see Ref. 3). In contrast, some tissues contain relatively large amounts of glycosphingolipids, for example in man, central and peripheral nerve myelin contains galactocerebroside as its major polar lipid [4]. The structural and/or functional role of galactocerebroside in myelin has not been determined. In addition, significant elevation of glycosphingolipids can occur in various tissues (brain, liver, spleen, etc.) as a result of inherited absences or defects of enzymes involved in glycosphingolipid degradation [5]. These pathological glycosphingolipidoses (and the accumulating glycosphingolipid) include gangliosidoses (G_{M1} and G_{M2} gangliosides), Fabry's disease (globosides), metachromatic leukodystrophy (cerebroside sulfate), Gaucher's disease (glucocerebroside), and Krabbe's disease (galactocerebroside).

The glycerolipids have been studied in detail by a variety of physical methods and a reasonably complete description of their structure and properties is available. Until recently, relatively few physical studies of sphingolipids (sphingomyelin and glycosphingolipids) had been made. Recent advances in the synthesis of sphingolipids of specific *N*-acyl-chain composition should allow more incisive studies of these membrane lipid components. For example, natural and homogeneously acylated sphingomyelins have been shown to form bilayer structures with thermotropic properties similar, but not identical, to the corresponding phosphatidylcholine [6–10].

For cerebrosides, their structure and properties have been studied by X-ray diffraction [11–15], calorimetric [15–20] and spectroscopic [21–24] methods .Notably X-ray diffraction [12] and single crystal [25] studies of synthetic cerebrosides by Pascher and colleagues have shown that cerebroside molecules pack in a bilayer arrangement, with the galactosyl groups aligned almost parallel to the membrane interface. A variety of hydrogen-bond donor and acceptor groups (>NH, –OH, >C=O) facilitate the formation of an extensive lateral hydrogen-bonded network involving the galactose and sphingosine moieties in the interfacial region. Our own studies have focused on the structure and properties of *N*-palmitoylgalactosylsphingosine (NPGS, galactocerebroside) and its interaction with phosphatidylcholine and cholesterol [15,26–28]. Hydrated NPGS exhibits complex polymorphic behavior, interconversions between stable and metastable bilayer structures, and a high-temperature (82°C), high-enthalpy (17.5 kcal/mol) bilayer-crystal to liquid-crystal transition [15]. This complex behavior has been attributed to variations in the hydrocarbon chain packing mode, the lateral H-bond interactions, and alterations in the hydration layer at the cerebroside bilayer interface [15]. Calorimetric studies suggest that glucocerebrosides exhibit similar thermotropic behavior, including low-temperature metastability [18]. Interestingly, the presence of 2-hydroxy fatty acid-containing cerebrosides seems to inhibit the low-temperature transition between metastable and stable forms [20].

It is well known that, in contrast to phospholipids, glycosphingolipids, including cerebrosides, have a significant amount of long-chain fatty acids (over 20 carbon atoms), in particular lignoceric ($C_{24:0}$) and nervonic ($C_{24:1}$) acids, *N*-acylated to the sphingosine base. It seems plausible that these long-chain membrane lipids may: (i) facilitate lateral phase separation of lipids, i.e., 'lipid patching'; (ii) prevent lipid desorption from the bilayer, i.e., 'anchoring', (iii) allow interaction between the two lipid monolayers of a membrane, i.e., 'communication'. Since our earlier studies of cerebrosides have focused on the shorter-chain *N*-palmitoyl derivative [15,26–28], we now describe our initial studies of the structure and properties of *N*-lignocerylgalactosylsphingosine (NLGS; galactocerebroside) using X-ray diffraction and calorimetric methods. Future studies will define its interactions with other lipids such as phosphatidylcholine and cholesterol, and perhaps in turn

allow the presence of long-chain glycosphingolipids in cell membranes to be rationalized.

Materials and Methods

Samples

NLGS was synthesized starting from pig brain cerebroside according to methods described by Skarjune and Oldfield [22], based on the original isolation, deacylation and reacylation procedures of Radin [29–31]. It is estimated that NLGS contains approx. 5% of the dihydrosphingosine derivative. By thin-layer chromatography, NLGS gave a single spot in the solvent system chloroform/methanol/water (65 : 25 : 4, v/v) and was used without further purification.

Differential scanning calorimetry

Hydrated multilamellar samples were prepared by weighing NLGS into stainless-steel pans, followed by the introduction of distilled water with a microsyringe to make approx. 70 wt% water dispersions. The pans were hermetically sealed and cycled between temperatures below and above the NLGS transition temperature (82°C, see below) to ensure equilibration. Heating and cooling scans were performed on a Perkin-Elmer (Norwalk, CT) DSC-2 with heating and cooling rates ranging from 0.625 to 80 Cdeg/min. Transition temperatures were determined by the position of the transition peak. Transition enthalpies were calculated by measuring the area under the peak with a planimeter, and comparison with those of a known gallium standard.

X-ray diffraction

Hydrated multilamellar samples were prepared by weighing NLGS into thin-walled (internal diameter = 1 mm) glass capillaries (Charles Supper Co., Natick, MA). Distilled water was added with a microsyringe to make a 70 wt% water dispersion of NLGS. For equilibration, the samples were centrifuged at room temperature to ensure that the NLGS and water had reached the bottom of the capillary, the capillary was flame sealed, and the sample was centrifuged approximately six times through the capillary at a temperature above that of the major phase transition (82°C, see below). The X-ray diffraction experiments were carried out with nickel-filtered CuK_α X-radiation ($\lambda = 1.5418$ Å) from an Elliot GX-6 rotating anode X-ray generator (Elliot Automation, Borehamwood, U.K.) and focused by a toroidal mirror optical camera. The samples were kept at constant temperature by a circulating ethylene glycol/water bath. For relatively fast cooling (about 2 Cdeg/min) the circulating solvent maintaining the high temperature was rapidly switched to an identical solvent maintained at a lower temperature. The sample temperature measured by a thermocouple adjacent to the sample was monitored continuously during this cooling period. The diffraction patterns were recorded on Kodak No-Screen X-ray film.

Results

Differential scanning calorimetry

The calorimetric behavior of hydrated (70 wt% water) NLGS is summarized in Fig. 1. Fig. 1A shows the initial heating run at 5 Cdeg/min following the equilibration procedure described in Materials and Methods. Three calorimetric transitions are observed on heating. The initial transition is endothermic and is centered at 69°C. The transition enthalpy is difficult to measure and is variable, due in part at least to the exotherm which follows. At 5 Cdeg/min a mean value of about 4 kcal/mol NLGS is obtained. This endotherm is followed immediately by an exothermic transition at 72°C, again with an enthalpy that is difficult to measure and is variable ($\Delta H \approx 2$ kcal/mol NLGS). The third transition is endothermic and represents the main phase transition of hydrated NLGS. This cooperative transition is centered at 82°C, with a transition enthalpy, ΔH of 15.3 kcal/mol NLGS. On cooling at 5 Cdeg/min, significant supercooling is observed (Fig. 1B). The initial exotherm occurs at 67°C, followed by a smaller peak at 65°C. The combined transition, transition I (onset 69°C to completion 58°C), has a total enthalpy $\Delta H = 6.0$ kcal/mol NLGS. A second exothermic transition, transition II, occurs at 45°C with a transition enthalpy $\Delta H = 8.1$ kcal/mol NLGS (Fig. 1b). Fig. 1C shows the DSC heating scan (5 Cdeg/min) performed immediately after completion of the cooling scan. Basically the same pattern of behavior is observed

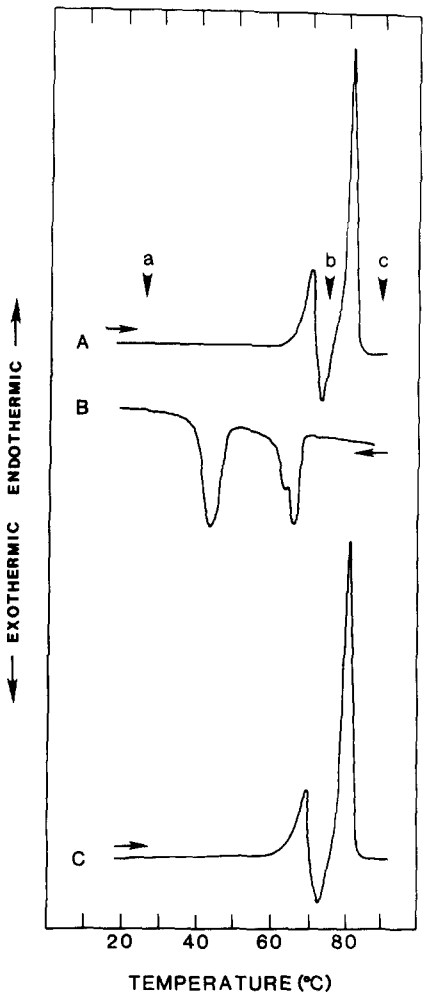

Fig. 1. DSC of hydrated (70 wt% H_2O) NLGS. (A) Heating curve, 5 Cdeg/min. (B) Cooling curve, 5 Cdeg/min. (C) Immediate re-heating curve, 5 Cdeg/min.

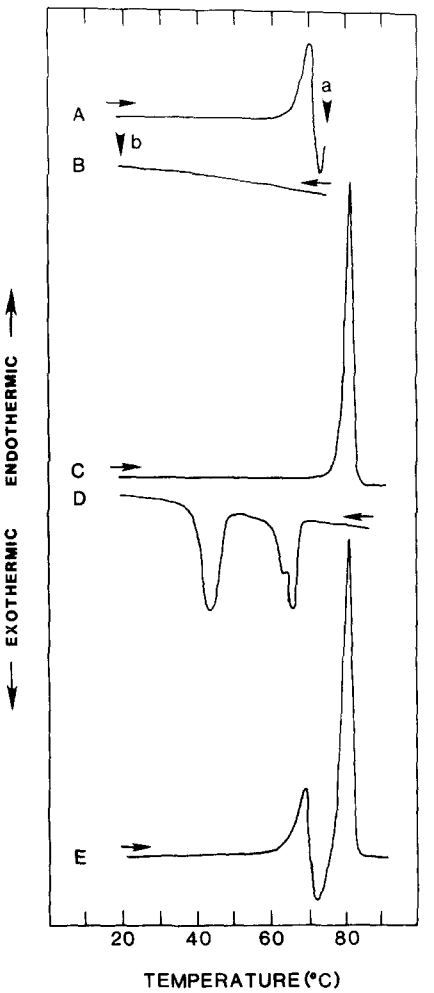

Fig. 2. DSC of hydrated (70 wt% H_2O) NLGS. (A) Heating curve to 77°C, 5 Cdeg/min. (B) Cooling curve, 5 Cdeg/min; following equilibration at 77°C for 1 h. (C) Immediate re-heating curve, 5 Cdeg/min. (D) Cooling curve, 5 Cdeg/min. (E) Immediate re-heating curve, 5 Cdeg/min.

as in the initial heating run, with the initial endotherm at about 70°C being followed immediately by the exotherm at about 73°C and finally, the high-enthalpy transition at 82°C. Some variability in the transition temperatures and enthalpies is observed for the low-temperature endotherm and exotherm at 69–70 and 72–73°C, respectively. The high-temperature endothermic transition is identical in both temperature (82°C) and enthalpy ($\Delta H = 15.3$ kcal/mol NLGS) to that observed in the initial heating scan (Fig. 1A). Repeated heating and cooling at 5 Cdeg/min shows behavior essentially identical to that shown in Fig. 1.

The reversibility of the complex endotherm-exotherm behavior at about 69–73°C was examined as shown in Fig. 2. Hydrated NLGS was heated at 5 Cdeg/min through both the initial endotherm at about 70°C and the exotherm at about 72°C and held at 77°C for 1 h (Fig. 2A). The subsequent cooling run following the 1 h incubation at 77°C shows no evidence of a thermal transition in the range 77 to 20°C (Fig. 2B). The following heating scan (Fig. 2C) confirms the irreversibility of the endothermic and exothermic behavior at about 70°C and 72°C, respectively. No transitions are

observed in this temperature range and only the high-temperature (82°C), high-enthalpy (ΔH = 15.3 kcal/mol NPGS) transition is observed (Fig. 2C). Heating through the high-temperature transition appears to be necessary for the subsequent characteristic exothermic behavior on cooling (Fig. 2D; see also Fig. 1B) performed immediately after the heating scan. The enthalpies associated with these transitions on cooling are 6.0 kcal/mol NLGS for the complex exotherm at about 66°C and 8.1 kcal/mol NLGS for the exotherm at about 45°C. Following this cooling run, immediate reheating at 5 Cdeg/min shows the reappearance of the endotherm at 69°C and the exotherm at 72°C, in addition to the high-temperature (82°C), high-enthalpy transition (Fig. 2E). Thus, the data presented in Fig. 2 indicate the following: (i) the endotherm-exotherm behavior at 69–73°C represents the endothermic conversion at about 70°C from a low-temperature NLGS form to a different form; this phase is thermodynamically unstable and immediately undergoes exothermic conversion at about 72°C to *the* stable form of NLGS; (ii) this phase of NLGS which undergoes the high-temperature (82°C), high-enthalpy (ΔH = 15.3 kcal/mol NLGS) transition is the stable form of NLGS in the temperature range 0–82°C, and all other low-temperature phases are metastable with respect to it; and (iii) only on cooling hydrated NLGS from the phase present at $T > 82$°C are the two transition exotherms (I and II) observed at about 65–67°C and about 45°C, resulting in the formation of the low-temperature NLGS phases (see below).

In order to derive more information about the phases formed on cooling and their stability, the complex exothermic transitions observed on cooling were studied as a function of cooling rate (Fig. 3A–G). At the fastest cooling rate recorded, 40 Cdeg/min, two exothermic transitions are observed at 57°C and 26°C. With decreasing cooling rate in the range 40 to 0.625 Cdeg/min, the low-temperature exotherm (transition II) occurs at progressively higher temperatures (26 to 58°C) and with progressively higher enthalpy (2.2 to 9.5 kcal/mol NLGS). The high-temperature exotherm (transition I) is much less dependent on cooling rate, increasing in temperature from 57 to 68°C (note also the resolution of the smaller peak

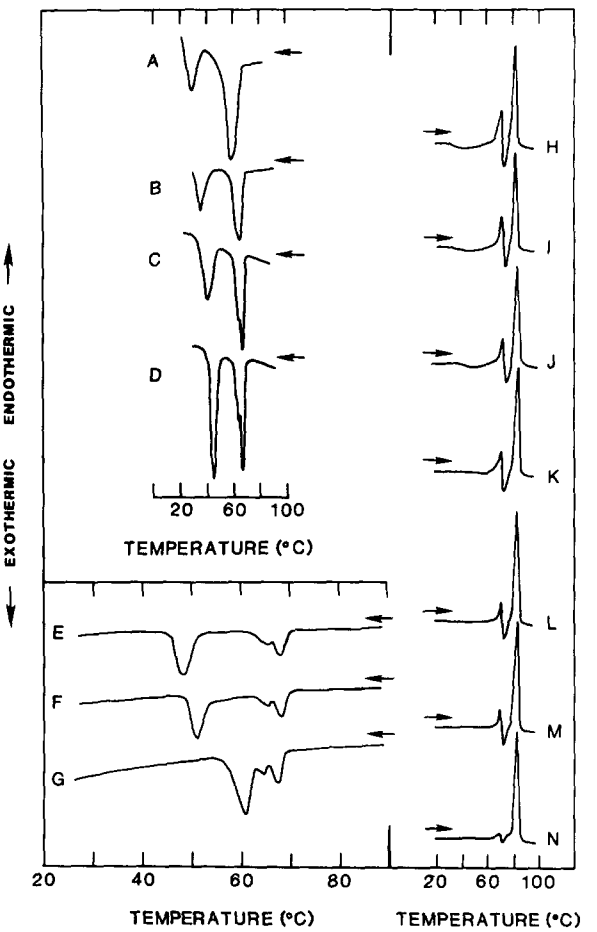

Fig. 3. DSC cooling curves of hydrated (70 wt% H_2O) NLGS at different cooling rates (40, 20, 10, 5, 2.5, 1.25 and 0.625 Cdeg/min, A–G). DSC heating curves (H–N, 5 Cdeg/min) immediately following cooling at 40, 20, 10, 5, 2.5, 1.25 and 0.625 Cdeg/min).

at about 65°C at lower cooling rates) with apparently a slight decrease in observed transition enthalpy (6.1 to 4.7 kcal/mol NLGS). This apparent decrease in enthalpy of transition I at the lowest cooling rate (0.625 Cdeg/min) is probably due to the lower signal-to-noise ratio and/or problems resolving the overlapped transitions I and II observed at this cooling rate (see Fig. 3G). The changes in transition temperature and enthalpy with cooling rate for the two exothermic transitions (I and II) are plotted in Fig. 4A and B, respectively. Following the cooling scan at 40 Cdeg/min showing a low-transition enthalpy for the exotherm at 26°C, the subsequent heating

scan at 5 Cdeg/min exhibits a broad exotherm centered at about 42°C prior to the 70°C (endotherm), 72°C (exotherm) and 82°C (endotherm) transitions (Fig. 3H). A similar exotherm at 42°C is observed following cooling at 20 and 10 Cdeg/min (Fig. 3I and J). At cooling rates no greater than 5 Cdeg/min, where the enthalpy associated with the low-transition exotherm (II) increases markedly (see Fig. 4B), no exothermic behavior is detectable at about 42°C on the subsequent heating run (Fig. 3K–N). In addition, the enthalpies associated with the endotherm and exotherm at 69 and 72°C decrease with decreasing prior cooling rate (Fig. 3H–N). After the lowest cooling rate (0.625 Cdeg/min; see Fig. 3G), most of the NLGS has converted to the stable form (T_m = 82°C) with only a small amount being present in the metastable phase exhibiting the endotherm-exotherm behavior at 69–72°C in the subsequent heating scan (see Fig. 3N). The approximate enthalpy (see comment above) of the transition endotherm (69°C) is plotted as a function of prior cooling rate in Fig. 4B. Clearly, the cooling rate 'independent' exotherm represents conversion of the high-temperature form to a metastable form, whereas the cooling-rate-dependent exotherms are associated with the formation of the stable phase of NLGS. At the lowest cooling rates the sum of transition enthalpies of exotherms I and II (plotted in Fig. 4B) reaches a value close to that of the 82°C endotherm observed on heating (i.e., 15.3 kcal/mol NLGS).

X-ray diffraction

In order to elucidate the structural changes of hydrated NLGS, X-ray diffraction patterns were recorded at different temperatures and following different equilibration conditions. The lettered arrows in Fig. 1 correspond to temperatures at which the X-ray diffraction patterns shown in Fig. 5 were recorded. Fig. 5 shows the initial X-ray diffraction pattern obtained at 26°C following

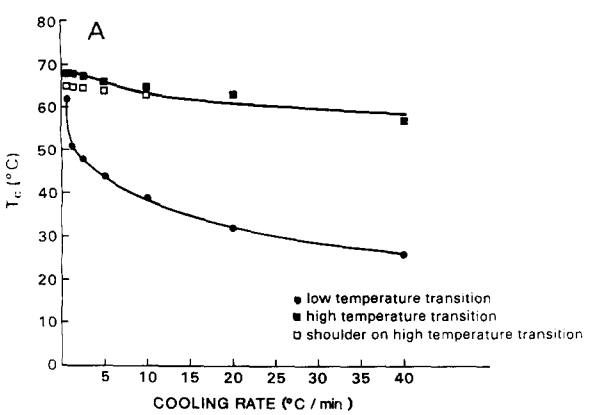

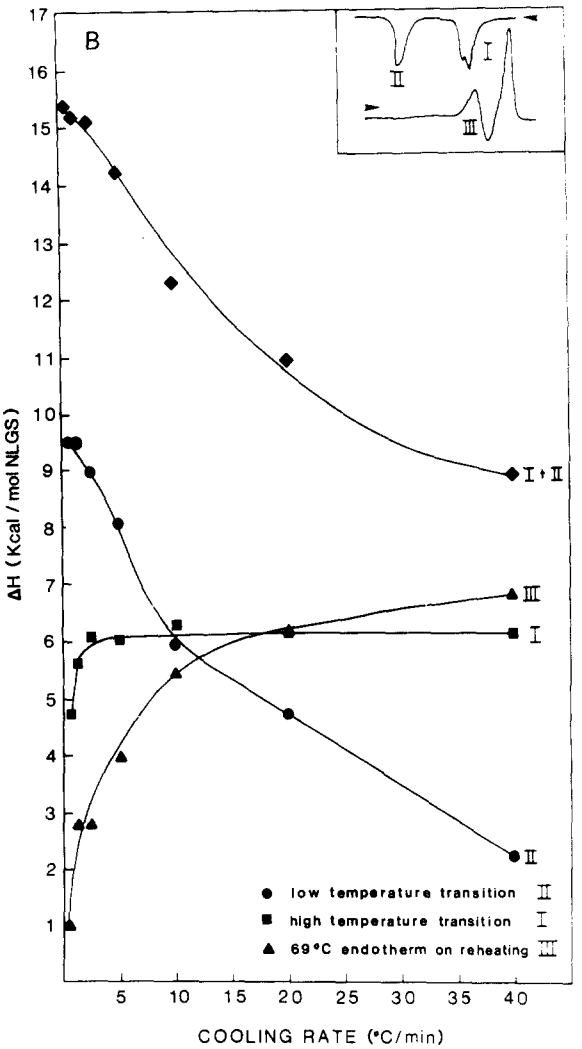

Fig. 4. (A) Transition temperatures of the exotherms observed on cooling hydrated (70 wt% H_2O) NLGS plotted as a function of cooling rate: ■, transition I; □, shoulder on transition 1; ●, transition II. (B) Transition enthalpies of the exotherms observed on cooling hydrated (70 wt% H_2O) NLGS; ■, transition I; ●, transition II; ◆, transitions I and II. The enthalpy of the endothermic transition at about 70°C on heating (transition III), following cooling at different rates, is also plotted, ▲.

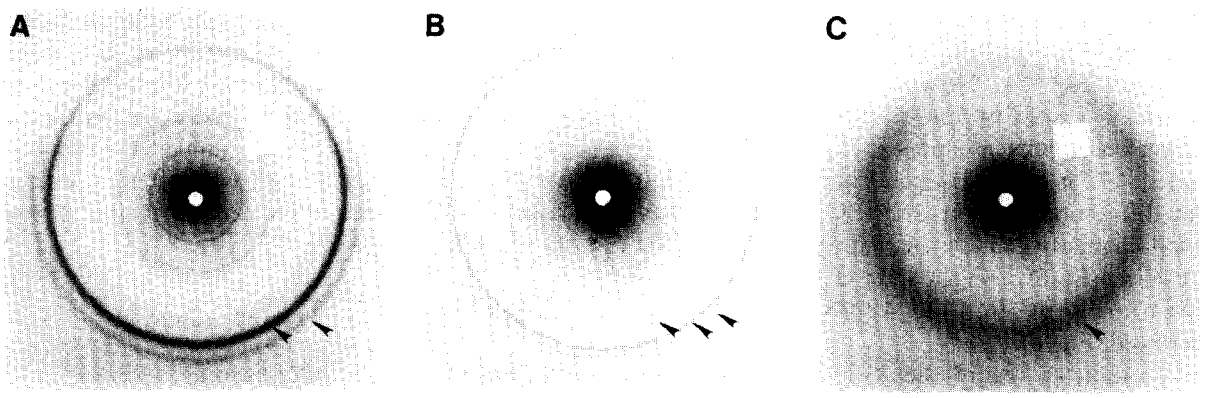

Fig. 5. X-ray diffraction patterns of hydrated (70 wt% H_2O) NLGS. (A) 26°C, following cooling from about 90°C at about 2 Cdeg/min (see text); (B) 75°C; (C) 93°C. Sample to film distance = 63.02 mm.

conventional equilibration conditions and a cooling rate of about 2 Cdeg/min from the high temperature phase (about 90°C) to 26°C (see Materials and Methods). A series of lamellar reflections ($h = 1$ to 7) are observed at low diffraction angles, corresponding to a bilayer periodicity (NLGS bilayer plus intercalated water), $d = 65.7 \pm 1.1$ Å. At higher diffraction angles, a number of diffraction lines are observed in the angular range 1/10 to 1/3 $Å^{-1}$, with the two strongest reflections appearing at 1/4.22 $Å^{-1}$ and 1/3.81 $Å^{-1}$ (arrowed, Fig. 5A). Additional weaker reflections are observed at 1/4.95, 1/5.03, 1/5.39, 1/8.08 and 1/9.43 $Å^{-1}$. The hydrated NLGS sample was then heated to 75°C, corresponding to a temperature above the initial endothermic and exothermic transitions (see Fig. 1A). The diffraction pattern (Fig. 5B) shows only minor changes in the positions and intensities of the low-angle reflections $h = 1$–8, with $d = 65.4 \pm 1.3$ Å. However, some changes in the wide-angle diffraction pattern are detectable, strong reflections being present at 1/4.1, 1/4.22 and 1/4.75 $Å^{-1}$ (arrowed, Fig. 5B; cf. Fig. 5A and 5B). Further heating to 93°C (above the high-temperature, high-enthalpy transition) results in the diffraction pattern shown in Fig. 5C. A series of lamellar reflections are observed in the low-angle region corresponding to a bilayer periodicity $d \cong 59.1$ Å and a broad diffuse reflection at about 1/4.6 $Å^{-1}$ (arrowed, Fig. 5C) is observed in the wide-angle region.

In a separate experiment, hydrated NLGS was heated to 75°C and its X-ray diffraction pattern was recorded (Fig. 6A). The lettered arrows in Fig. 2 correspond to temperatures at which the X-ray diffraction pattern in Fig. 6 were recorded. This diffraction pattern is identical to that at 75°C described above (Fig. 5B). The sample was then

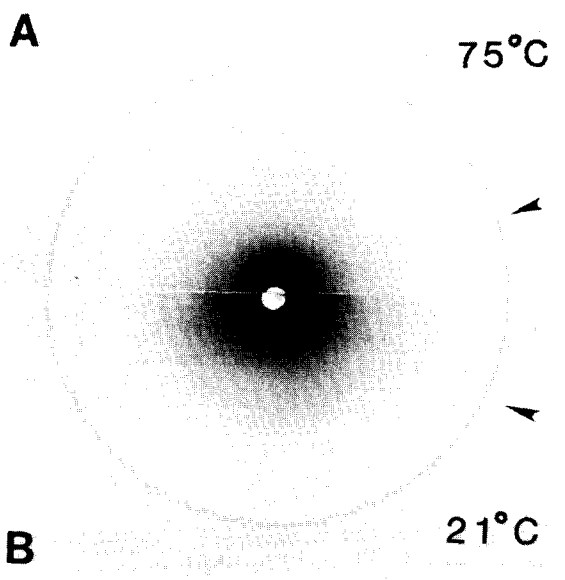

Fig. 6. X-ray diffraction patterns of hydrated (70 wt% H_2O) NLGS. (A) At 75°C, following heating. (B) At 21°C, following cooling from 75°C, see (A). Sample to film distance = 63.02 mm.

cooled to 21°C (for the equivalent DSC experiment, see Fig. 2) and the diffraction pattern was recorded (Fig. 6B). No significant changes occur in the low-angle region ($d = 65.0 \pm 1.3$ Å) and strong reflections are present at 1/3.90, 1/4.19 and 1/4.77 in the wide-angle region. Compared to the diffraction pattern at 75°C, only relatively small changes occur in the wide-angle region, the most significant being a shift in the reflection at 1/4.10 $Å^{-1}$ at 74°C to 1/3.90 $Å^{-1}$ at 21°C (arrowed, Fig. 6).

Attempts to record the X-ray diffraction pattern of hydrated NLGS exclusively in the metastable low-temperature phase either at about 20 or 55°C have not been successful due to difficulties in achieving the fast cooling rate (over 10 Cdeg/min) required to limit formation of the stable phase (see Fig. 3) and/or to the rather long acquisition time required to record the diffraction pattern (during which conversion of the metastable phase to the stable phase occurs). In most cases, a diffraction pattern similar to that shown in Fig. 5A is observed.

Discussion

Thermotropic properties of hydrated NLGS

On heating, hydrated NLGS exhibits a complex pattern of thermotropic behavior. Three transitions are observed on heating; two variable-en-

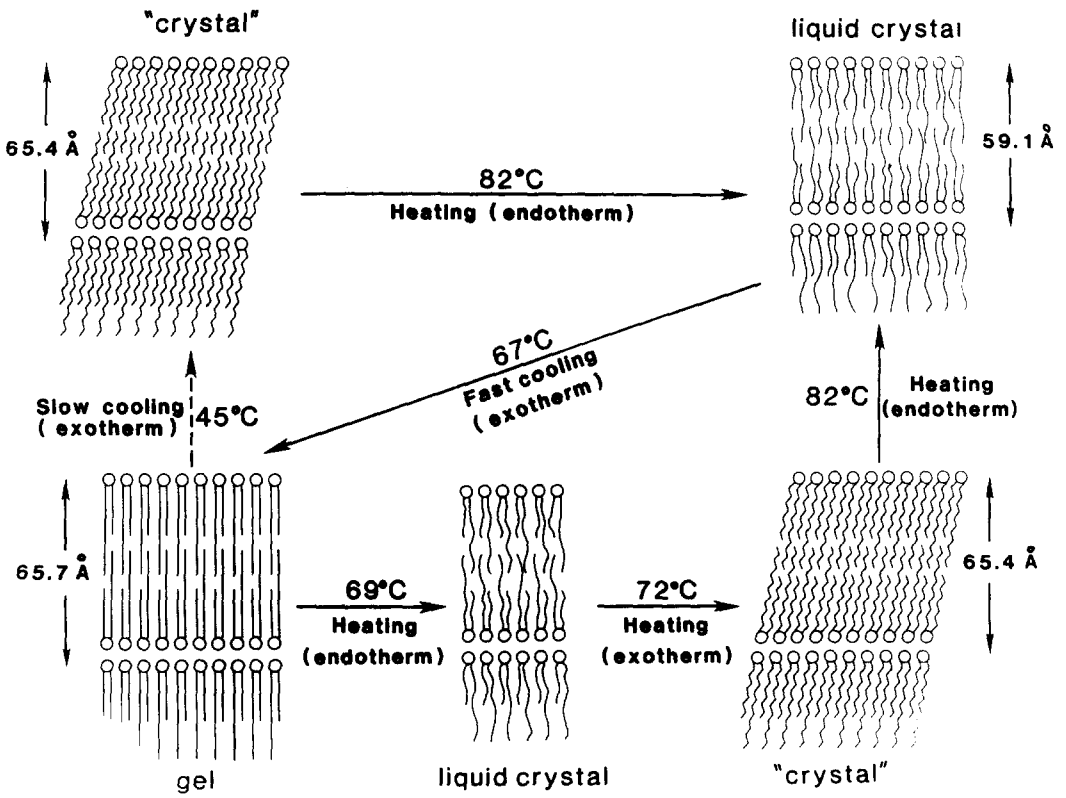

Fig. 7. Schematic representation of the bilayer structures and thermotropic behavior of hydrated NLGS. The stable 'crystal' bilayer phase is represented with zig-zag chains, indicating a highly ordered chain-packing mode (see text). The gel bilayer phase is represented with straight chains, indicating the rotationally disordered, hexagonally packed chain packing mode (see text). The precise tilt with respect to bilayer normal is not known and the molecules are shown in an untilted form. The liquid crystal bilayer phase is represented with wavy chains indicative of the melted chain conformation and the presence of *gauche* isomers along the chains. Since the presence of the liquid crystal bilayer intermediate between the gel and crystal bilayer forms (bottom) has not been 'trapped', no molecular information on its structure is available.

thalpy transitions at 69°C (endotherm) and 72°C (exotherm), followed by an invariable transition ($\Delta H = 15.3$ kcal/mol NLGS) at 82°C. This complexity is due to the presence of metastable and stable low-temperature forms and is strongly influenced by the prior thermal treatment of NLGS. It is simpler to consider first the behavior of hydrated NLGS on cooling from the high-temperature phase (for a summary, see Fig. 7). Above the high-temperature (82°C), high-enthalpy ($\Delta H = 15.3$ kcal/mol NLGS) transition, the X-ray diffraction data confirm that NLGS forms a hydrated lamellar phase, of bilayer periodicity 59.1 Å. The hydrocarbon chains are clearly in the melted configuration, as revealed by the broad reflection at 1/4.6 $Å^{-1}$. This X-ray diffraction pattern resembles that of other hydrated liquid-crystalline bilayers (L_α) formed by phospholipids, glycolipids, etc.

On cooling, the L_α phase of hydrated NLGS exhibits significant supercooling; even at the lowest cooling rate (0.625 Cdeg/min) the onset of the first exothermic transition (I) does not occur until 70°C. Neither the temperature nor the enthalpy of this exothermic transition is significantly influenced by the cooling rate, except perhaps at the lowest cooling rates (Fig. 4). The enthalpy of this transition is about 6 kcal/mol NLGS, a value less than half that exhibited at the 82°C transition on heating. This transition enthalpy is similar to that exhibited by hydrated phospholipid bilayers undergoing bilayer liquid crystal to bilayer gel ($L_\alpha \rightarrow L_\beta$) transitions, where the gel phase (L_β or $L_{\beta'}$) has the hydrocarbon chains packed in an hexagonal arrangement (for examples, see Refs. 6,8–11,32–37). Attempts to record the X-ray diffraction pattern of only this phase of NLGS have not been successful (see Results). However, the diffraction pattern recorded in the presence of the stable phase suggests that the bilayer periodicity does not differ greatly from that of the stable phase, i.e., about 65 Å. Thus, on cooling NLGS from the L_α phase we suggest that the initial phase formed is a bilayer gel structure (L_β or $L_{\beta'}$) with hexagonally packed chains (see Fig. 7). The presence of a strong, rather broad reflection at 1/4.22 $Å^{-1}$ at 26°C is consistent with the presence of a gel phase at this temperature (see Fig. 5A).

On further cooling, hydrated NLGS exhibits a second exothermic transition (II) with a transition temperature and enthalpy that is markedly dependent on cooling rate. At the lowest cooling rate most of the intermediate bilayer gel phase (L_β) converts to a different low-temperature phase. With progressively higher cooling rates, less of the NLGS is converted and this remains as the L_β phase at low temperatures. Thus, depending on the cooling rate, differing amounts of the two phases will be present at low temperatures. The two co-existing phases present at low temperatures following cooling exhibit different thermotropic behavior (see Fig. 7). The 'unconverted' metastable gel form of NLGS exhibits the endothermic transition at about 69°C followed by the exothermic transition at about 72°C, representing the conversion of the metastable gel phase to the stable low-temperature form, the latter being identical to that produced by exothermic transition II on cooling. Again, based on enthalpy arguments we believe that the metastable L_β bilayer phase undergoes an endothermic hydrocarbon chain melting transition at 69°C to produce a melted chain L_α bilayer phase. This phase is also metastable at this temperature and immediately converts exothermically at 72°C to the stable, high-melting (82°C) NLGS phase.

Using the protocol shown in Fig. 2 we have converted all the NLGS into the stable form and thus we have been able to record the X-ray diffraction pattern of only the stable form. Clearly, the stable, low-temperature phase of hydrated NLGS is a lamellar structure with a bilayer periodicity of 65.4 Å. The presence of numerous sharp reflections in the wide-angle region show that this is not a simple gel phase with hexagonally packed chains. Rather, the diffraction pattern indicates the presence of a bilayer phase in which the hydrocarbon chains have adopted one of the specific crystalline chain-packing arrangements defined by either a simple or a complex sub-cell [38–40]. We refer to this as a stable 'crystal' bilayer (see Fig. 7). This crystal bilayer phase represents the stable form of hydrated NLGS over the temperature range 0–82°C.

At 82°C, the stable crystal bilayer form of NLGS converts to the melted-chain L_α bilayer phase (see Fig. 7). The large enthalpy is a result of

the energy requirements to melt hydrocarbon chains packed in a crystalline lattice.

Comparison with other glycosphingolipids

(a) Structural considerations. From the crystal structure analysis of 2-*D*-hydroxystearoylgalactosyldihydrosphingosine [25], a bilayer length of 61 Å is calculated for this C_{18} cerebroside. Assuming the molecular conformation is similar for NPGS, C_{16} cerebroside, and remembering that the sphingosine chain is invariant, a bilayer molecular length of 61–2.5 Å = 58.5 Å is calculated. The observed bilayer periodicity of the stable E phase of NPGS is 54.5 Å [15]. If, as we suspect [15,26], this phase is not extensively hydrated, the water layer thickness may be negligible. With this assumption we calculate a molecular tilt angle of 21° with respect to the bilayer normal for NPGS. For the stable phase of NLGS the wide-angle diffraction pattern is similar to that of NPGS described above [15] and thus a similar bilayer structural arrangement is expected. Assuming that the tilt angle is identical to that of NPGS, i.e., 21°, and that the water layer thickness is negligible, the bilayer periodicity of NLGS, 65.0 Å, can be used to calculate the bilayer molecular length of 69.6 Å. This is in good agreement with the bilayer length (68.5 Å) calculated assuming partial chain interdigitation, the C_{24} chain on one side of the bilayer being apposed with the sphingosine chain on the other side of the bilayer, and vice versa, as shown in Fig. 7 ('crystal'). Although dependent on a number of assumptions, the X-ray diffraction data suggest that partial chain interdigitation occurs in the stable bilayer phase of NLGS.

For the melted chain, L_α bilayer phase which for NPGS, at least, does have a significant hydration contribution to the bilayer thickness (Ruocco and Shipley, unpublished data), the increase in bilayer thickness in going from C_{16} (NPGS; $d = 51$ Å) to C_{24} (NLGS; $d = 59$ Å) is 8 Å. With the assumption that this increment is due primarily to a change in the bilayer thickness and not the hydration thickness, this value is consistent with a partially interdigitated arrangement of the melted chains as indicated in Fig. 7 ('liquid crystal').

(b) Thermotropic behavior. Previous studies of *N*-palmitoyl galactosylsphingosine (NPGS) in which the sphingosine and *N*-acyl chains are more evenly matched than in NLGS, also demonstrated a complex polymorphic behavior [15] which differed markedly from that of membrane phospholipids. Hydrated NLGS and NPGS both exhibit high temperature (NLGS, 82°C; NPGS, 82°C), high enthalpy (NLGS, $\Delta H = 15.3$ kcal/mol; NPGS, $\Delta H = 17.5$ kcal/mol) transitions from ordered chain, crystalline bilayer phases to melted chain L_α bilayer phases. The behavior on cooling appears similar for NLGS and NPGS in that both exhibit two distinct exothermic transitions as the cerebrosides form first a metastable bilayer phase (for NPGS, anhydrous crystal A form, see Ref. 15), and then a stable hydrated bilayer phase (for NPGS, crystal form E, see Ref. 15). The dependence of these two transitions on cooling rate is qualitatively similar for both NLGS and NPGS, with the higher-temperature transition being cooling-rate-independent and the lower-temperature transition being cooling-rate-dependent in both cases. For NPGS we were able to record the diffraction pattern of the metastable phase and to show that this was an anhydrous NPGS bilayer phase [15]. On heating, this metastable phase exhibited an exothermic transition at about 52°C to the hydrated stable, crystal E bilayer phase. For NLGS we have not been able to 'trap' and define the structure of the corresponding metastable phase. However, on heating, the metastable phase of NLGS exhibits behavior slightly different from that of the previously characterized NPGS [15]. Notably, only following very rapid cooling does NLGS exhibit an exothermic transition on heating at about 40–50°C (see Fig. 3H–J). This exotherm probably represents the conversion of a dehydrated NLGS phase (formed only at the very high cooling rates) to the stable hydrated bilayer form of NLGS which then undergoes the high temperature transition (i.e., analogous to the behavior of NPGS, see Ref. 15). We have not studied the structural basis for this exotherm. In contrast, following slower cooling no exothermic behavior is observed at temperatures under 60°C; instead the metastable form exhibits an endothermic transition at 69°C, immediately followed by an exotherm at 72°C. We suggest that this metastable form of NLGS is a hydrated bilayer, perhaps with hexagonally packed chains (see strong 1/4.2 $Å^{-1}$ reflection, Fig. 5A), which

undergoes a relatively low-enthalpy, endothermic bilayer gel → bilayer liquid-crystal (L_α) transition at 69°C. The difference between the hydrated metastable form and the stable state lies, in part at least, in the differences in the chain packing. The metastable form probably has hexagonally packed chains, while the stable form has a highly ordered chain-packing mode corresponding to a specific sub-cell arrangement. Since the L_α phase is metastable with respect to the stable, high-melting form it converts to the stable form exothermically at about 72°C.

Thus, although NLGS and NPGS show similar thermotropic behavior, they appear to differ in temrs of the kinetics of bilayer dehydration-hydration processes. So far we have not been able to define the contribution of the marked asymmetry in chain length of NLGS to its thermotropic behavior.

Recent studies by Curatolo [20,41] on isolated hydroxy- and non-hydroxy fatty acid subfractions of bovine brain cerebrosides show similarities with the behavior of the synthetic NLGS described here and NPGS [15]. Of note is the effect of a 2-hydroxy fatty acid in cerebrosides which appears to prevent the formation of the stable phase and considerably simplifies the low-temperature polymorphic behavior of cerebrosides [20,41]. Finally, Boggs and co-workers [42,43] have studied the thermotropic properties of synthetic sulfatides (cerebroside 3-sulfate). These negatively charged sulfatides show thermal characteristics similar, but not identical, to those of the related cerebrosides. In particular, sulfatides also appear to show conversions between metastable and stable states on cooling [42,43].

Acknowledgements

We thank Drs. E. Oldfield and R.P. Skarjune for supplying NLGS. We acknowledge useful discussions with Drs. M.J. Ruocco and D. Atkinson, and technical assistance from D. Jackson. We thank Irene Miller for help in the preparation of this manuscript. This work was supported by National Institutes of Health research grant HL-26335 and training grants HL-07291 and HL-07429.

References

1 Rouser, G., Nelson, G.J., Fleischer, S. and Simon, G. (1968) in Biological Membranes, Chapman, D., ed.), pp. 5–69, Academic Press, New York
2 Linington, C. and Rumsby, M.G. (1978) Adv. Exp. Med. Biol. 100, 263–273
3 Hakomori, S.I. (1981) Annu. Rev. Biochem. 50, 733–764
4 Rumsby, M.G. (1978) Biochem. Soc. Trans. 6, 448–462
5 Fishman, P.H. and Brady, R.O. (1976) Science 194, 906–915
6 Shipley, G.G., Avecilla, L.S. and Small, D.M. (1974) J. Lipid Res. 15, 124–131
7 Barenholz, Y., Suurkuusk, J., Mountcastle, D., Thompson, T.E. and Biltonen, R.L. (1976) Biochemistry 15, 2441–2447
8 Calhoun, W.I. and Shipley, G.G. (1979) Biochemistry 18, 1717–1722
9 Estep, T.N., Calhoun, W.I., Barenholz, Y., Biltonen, R.L., Shipley, G.G. and Thompson, T.E. (1980) Biochemistry 19, 20–24
10 Maulik, P.R., Scripada, P.K. and Shipley, G.G. (1985) Biophys. J. 47, 44a
11 Reiss-Husson, F. (1967) J. Mol. Biol. 25, 363–382
12 Abrahamsson, S., Pascher, I., Larsson, K. and Karlsson, K.-A. (1972) Chem. Phys. Lipids 8, 152–179
13 Fernandez-Bermudez, S., Loboda-Cackovic, J., Cackovic, H. and Hosemann, R. (1977) Z. Naturforsch. C 32, 362–374
14 Hosemann, R., Loboda-Cackovic, J. and Cackovic, H. (1979) Z. Naturforsch. C 34, 1121–1124
15 Ruocco, M.J., Atkinson, D., Small, D.M., Skarjune, R.P., Oldfield, E. and Shipley, G.G. (1981) Biochemistry 20, 5957–5966
16 Clowes, A.W., Cherry, R.J. and Chapman, D. (1971) Biochim. Biophys. Acta 249, 301–317
17 Bunow, M.R. (1979) Biochim. Biophys. Acta 574, 542–546
18 Freire, E., Bach, D., Correa-Freire, M., Miller, I. and Barenholz, Y. (1980) Biochemistry 19, 3662–3665
19 Linington, C. and Rumsby, M.G. (1981) Neurochem. Int. 3, 211–218
20 Curatolo, W. (1982) Biochemistry 21, 1761–1764
21 Bunow, M.R. and Levin, I.W. (1980) Biophys. J. 32, 1007–1021
22 Skarjune, R. and Oldfield, E. (1979) Biochim. Biophys. Acta 556, 208–218
23 Skarjune, R. and Oldfield, E. (1982) Biochemistry 21, 3154–3160
24 Huang, T.H., Skarjune, R.P., Wittebort, R.J., Griffin, R.G. and Oldfield, E. (1980) J. Am. Chem. Soc. 102, 7377–7379
25 Pascher, I. and Sundell, S. (1977) Chem. Phys. Lipids 20, 175–191
26 Ruocco, M.J. and Shipley, G.G. (1983) Biochim. Biophys. Acta 735, 305–308
27 Ruocco, M.J., Shipley, G.G. and Oldfield, E. (1983) Biophys. J. 43, 91–101
28 Ruocco, M.J. and Shipley, G.G. (1984) Biophys. J. 46, 695–707
29 Radin, N.S. (1976) J. Lipid Res. 17, 290–293
30 Radin, N.S. (1972) Methods Enzymol. 28, 300–306
31 Radin, N.S. (1974) Lipids 9, 358–360

32 Chapman, D., Williams, R.M. and Ladbrooke, B.D. (1967) Chem. Phys. Lipids 1, 445–475
33 Janiak, M.J., Small, D.M. and Shipley, G.G. (1976) Biochemistry 15, 4575–4580
34 Janiak, M.J., Small, D.M. and Shipley, G.G. (1979) J. Biol. Chem. 254, 6068–6078
35 Ruocco, M.J. and Shipley, G.G. (1982) Biochim. Biophys. Acta 684, 59–66
36 Mulukutla, S. and Shipley, G.G. (1984) Biochemistry 23, 2514–2519
37 Hauser, H., Paltauf, F. and Shipley, G.G. (1982) Biochemistry 21, 1061–1067
38 Abrahamsson, S., Dahlen, B., Lofgren, H. and Pascher, I. (1978) Prog. Chem. Fats Other Lipids 16, 125–143
39 Shipley, G.G. (1986) in Handbook of Lipid Research, Vol. 4 (Small, D.M., ed.), pp. 97–147, Plenum Press, New York
40 Ruocco, M.J. and Shipley, G.G. (1982) Biochim. Biophys. Acta 691, 309–320
41 Curatolo, W. and Jungalwala, F.B. (1985) Biochemistry 24, 6608–6613
42 Koshy, K.M. and Boggs, J.M. (1983) Chem. Phys. Lipids 34, 41–53
43 Boggs, J.M., Koshy, K.M. and Rangaraj, G. (1984) Chem. Phys. Lipids 36, 65–89